Spectroscopic and Photothermal Study of Myoglobin Conformational Changes in the Presence of Sodium Dodecyl Sulfate

Jaroslava Mikšovská,*,† Jenny Yom,† Brian Diamond,† and Randy W. Larsen‡

Chemistry Department, Marshall University, Huntington, West Virginia 25755, and Chemistry Department, University of South Florida, Tampa Florida 42021

Received September 12, 2005; Revised Manuscript Received November 22, 2005

Interactions between sodium dodecyl sulfate (SDS) and horse heart myoglobin (Mb) at surfactant concentrations below the critical micelle concentration have been studied using steady-state and transient absorption spectroscopies and photoacoustic calorimetry. SDS binding to Mb induces a heme transition from high-spin five-coordinate to low-spin six-coordinate in met- and deoxyMb, with the distal His residue likely to be the sixth ligand. The transition is complete at an SDS concentration of ~350 μM and ~700 μM for met- and deoxyMb, respectively. ΔG_{H_2O} and *m* values determined from equilibrium SDS-induced unfolding curves indicate similar stability of met- and deoxyMb toward unfolding; however, the larger *m* value for the deoxyMb equilibrium intermediate indicates that its structure differs from that of metMb. Results from transient absorption spectroscopy show that CO rebinding to Fe^{2+}−Mb in the presence of SDS is a biphasic process with the rate constant of the first process approximately 5.5×10^3 s^{-1}, whereas the second process displays a rate similar to that for CO rebinding to native Mb ($k_{obs} = 7.14 \times 10^2$ s^{-1}) at 1 mM CO. Results of photoacoustic calorimetry show that CO dissociation from deoxyMb occurs more than 10 times faster in the presence of SDS than in native Mb. These data suggest that the heme binding pocket is more solvent-exposed in the SDS-induced equilibrium intermediate relative to native Mb, which is likely due to the electrostatic and hydrophobic interactions between surfactant molecules and the protein matrix.

Introduction

Surfactants are widely employed in biochemistry and biotechnology for the purpose of protein solubilization, purification, characterization, and protein structure determination.[1,2] Mild surfactants are often used to extract membrane proteins while preserving their native structure and functional properties, whereas strong ionic surfactants are known to bind to oppositely charged protein molecules, resulting in denaturation of the native structure and complete loss of protein activity.[3] For example, the commonly used anionic surfactant sodium dodecyl sulfate (SDS) is known to destabilize several proteins even at the millimolar level. Complete understanding of the effect of surfactants on protein structure requires detailed characterization of protein−surfactant complexes at various surfactant concentrations.[4]

The interactions between SDS and globular proteins such as bovine serum albumin and lysozyme have been extensively investigated in terms of binding isotherms. These studies have led to a suggestion that, at low surfactant concentration, SDS binds specifically and noncooperatively, while an increase in the SDS concentration is associated with nonspecific and cooperative binding. Hydrophobic and electrostatic interactions are believed to be involved in the specific binding, whereas nonspecific interactions are likely to be dominated by hydrophobic forces.[5] Protein denaturation is likely to occur during the cooperative phase of surfactant binding. Different models have been proposed to describe saturated protein−SDS complexes, including the α-helix/random coil model, necklace model, rodlike particle model, and flexible helix model.[6] However, recent NMR results and small angle neutron scattering studies support the "necklace model", where micelle-like aggregates are formed along the protein chain.[7,8]

Despite the fact that the binding characteristics of SDS to water-soluble proteins have been well-established and several studies have suggested alteration of secondary and tertiary structure along binding isotherms, significantly less is known about protein−surfactant interactions on the molecular level. Heme proteins, such as cytochrome *c* and myoglobin, are well-suited model systems for monitoring protein−surfactant interactions, because the physical properties of these proteins have been well-characterized and conformational changes can be monitored using a variety of spectroscopic techniques. SDS-induced cytochrome *c* unfolding has been investigated using fluorescence, resonance Raman spectroscopy, and NMR.[5,9,10] From these studies, it was suggested that, in the presence of SDS, horse heart cytochrome *c* undergoes a conformational transition associated with the cleavage of the Fe−Met 80 bond and an accumulation of a non-native bis His intermediate.[9] Changes in heme iron coordination in the presence of SDS have also been observed in NMR studies of yeast iso-1 cytochrome *c* at 100 mM SDS, and the presence of a high-spin species with a detached Met 80 and a low-spin six-coordinate species having a His residue in the position of the distal ligand was reported.[10] On the other hand, SDS also induces refolding of acid-denatured cytochrome *c* in a molten globule-like equilibrium state, and the molten globule state can be achieved at very low SDS concentration as well as above the critical micelle concentration (cmc) value.[11,12]

Similarly, Sau et al.[13] reported that SDS at a concentration range below the cmc converts human native and cross-linked high-spin Fe^{3+} hemoglobin into six-coordinate low-spin Fe^{3+} hemoglobin with two histidine residues in the axial ligand

† Marshall University.
‡ University of South Florida.

10.1021/bm0506703 CCC: $33.50
Published on Web 01/06/2006

positions. These authors suggested that SDS binding to hemoglobin induces a conformational change within the heme binding pocket that may result in the binding of the distal histidine to the heme iron. Recently, Tofani et al.[14] have investigated interactions between myoglobin and several surfactant molecules using steady-state absorption and fluorescent spectroscopy. These authors reported that SDS molecules specifically bind to metmyoglobin, resulting in an increase in protein flexibility and the formation of a six-coordinate myoglobin with a histidine residue as a distal ligand.

Characterization of CO binding kinetics to heme iron has previously been shown to provide useful information regarding the structure and dynamics of heme base proteins/enzymes including myoglobin, hemoglobin, and cytochrome P_{450}.[15] With this in mind, we have employed transient absorption spectroscopy and photoacoustic calorimetry (PAC) to determine the kinetics and the magnitudes of molar volume and enthalpy changes coupled to ligand dissociation and rebinding to deoxymyoglobin in the presence of SDS at concentrations below the cmc.

Materials and Methods

Horse heart myoglobin (Mb), sodium dodecyl sulfate, Tris buffer, and sodium dithionite were purchased from Sigma-Aldrich and used as received. Fe(III) tetrakis(4-sulfonatophenyl)porphine was purchased from Porphyrin Products Inc. Samples were prepared by dissolving Mb in 50 mM Tris buffer, pH 7.5. The cuvette was then sealed with a septum cap and purged with Ar for ~20 min. A small addition of sodium dithionite was used to reduce the sample. Finally, the sample was flushed with CO for approximately 5 min. Formation of deoxyMb and CO-bound Mb was verified from steady-state optical spectra measured using a single beam UV−vis spectrophotometer (Carry 50, Varian).

SDS titrations were carried out by monitoring optical spectra between 350 and 700 nm upon addition of small aliquots of SDS (1 μL of 0.1 M stock SDS) to a 2 mL sample of 5 μM met- or deoxyMb. The unfolding transitions at 25 °C were analyzed in terms of a two-state model as presented by Santoro and Bolen[16]

$$y = \{(\Delta\theta_N + m_N[D]) + (\Delta\theta_U + m_U[D])\exp[-(\Delta G_{H_2O}/RT + m[D]/RT)]\}/\{1 + \exp[-(\Delta G_{H_2O}/RT + m[D]/RT)]\} \quad (1)$$

where [D] is the denaturant concentration and $\Delta\theta_N$, $\Delta\theta_U$, m_N, and m_U are the fitting parameters. $\Delta\theta_N$ and $\Delta\theta_U$ are the observable values of the native and fully unfolded protein at zero denaturant concentration, respectively, and m_N and m_U represent their respective dependence on denaturant concentration, the slope of the pre- and post-folding baselines, respectively. The free energy of unfolding (ΔG_{H_2O}) and equilibrium m value are the intercept and the slope, respectively, of the linear extrapolation of the unfolding free energy changes versus denaturant concentration. The midpoint of the transition (C_m) was obtained by fitting a four-parameter sigmoidal equation (Microcal Origin, version 5.0) to the fraction of unfolded protein as a function of SDS concentration.

The CO association constant was determined by a spectrometric titration. Titrations were performed by sequentially adding saturated aqueous CO to a solution of 5 μM Mb reduced by a small addition of sodium dithionite in 50 mM Tris buffer, pH 7.5, and 700 μM SDS. Absorbance changes were recorded in the spectral region between 350 and 700 nm. The association constant (K_a) was found by assuming a simple two-step equilibrium: CO + Fe(II)Mb ↔ (CO)Fe(II)Mb. The change in absorbance as a function of CO concentration then allows for the determination of K_a from

$$\Delta A = \frac{K_a \Delta\epsilon c[CO]}{1 + K_a[CO]} \quad (2)$$

where $\Delta\epsilon$ is the change in the molar extinction coefficient at the monitoring wavelength, c is the initial concentration of Mb, and [CO] is the solution concentration of CO.

CO rebinding kinetics were studied using a home-built transient absorption instrument. The probe beam from a 150 W Xe arc lamp (Thermo-Oriel) was centered on the sample housed in a Quantum Northwest 1 cm variable temperature cell holder, and the emerging light was then focused on the slit of a monochromator (Micro HR, Jobin Yvon) and detected by a PMT (H6780, Spectra-Physics) coupled to a high-gain amplifier (70710, Spectra-Physics). The signal was then digitized using a 100 MHz transient digitizer (TDS 2012, Tektronix). The photochemistry was initiated by a 532 nm pulse from a frequency-doubled Nd:YAG laser (Minilite II, Continuum), 7 ns pulse width, 1 Hz repetition. Data were fitted by either one or two exponential decay functions using Microcal Origin, version 5.0.

The photoacoustic setup and analysis have been described in detail elsewhere.[17−19] Briefly, CO-bound Mb samples for photoacoustic measurements were prepared as described above and contained approximately 20 μM Mb in a 1 cm quartz cuvette. The sample was placed in a temperature-controlled cuvette holder (Quantum Northwest) with a 1 MHz photoacoustic detector (TR−V103, Panametrics) mounted on the cuvette side. The coupling between the cuvette and the detector was facilitated by a thin layer of vacuum grease. The signal was amplified using a Panametrics 5662 preamplifier and fed into a 500 MHz digitizer (TDS 544A, Tektronix). Ligand photodissociation was achieved by a 532 nm pulse from a frequency-doubled Nd:YAG laser (7 ns pulse, Minilite II, Continuum). The pulse energy was kept below 50 μJ to prevent a multiphoton absorption. In general, 30 traces were averaged to improve the signal-to-noise ratio. The reaction volume (ΔV) and enthalpy changes (ΔH) are determined from a plot of the ratio of amplitudes of the sample acoustic signal to the reference signal versus the thermoelastic parameters of the solution ($C_p\rho/\beta$) according to[19]

$$\frac{S}{R}E_{h\nu} = Q + \Delta V'\frac{C_p\rho}{\beta} \quad (3)$$

$$\Delta H = \frac{E_{h\nu} - Q}{\Phi} \quad (4)$$

$$\Delta V = \frac{\Delta V'}{\Phi} \quad (5)$$

where S and R are the amplitude of the acoustic wave for the sample and the reference, respectively, $E_{h\nu}$ is the energy of the photon at 532 nm (53.7 kcal mol^{-1}), Q is the amount of heat released to the solution, $\Delta V'$ is the volume change per photon absorbed, C_p is the heat capacity, ρ is the density, β is the thermal expansion coefficient, and Φ is the quantum yield.

Results

Figure 1 displays the steady-state optical spectra of Mb in the presence of SDS. Titration of metMb with SDS causes a red shift of the Soret band to 414 nm, a diminishing of the 504 nm band, and the appearance of two new bands situated at 535 and 567 nm. The 634 nm band characteristic of the high-spin ferric heme species disappears. In the case of deoxyMb, the addition of SDS leads to a blue shift of the Soret band to 427 nm and the appearance of α and β bands at 560 and 530 nm, respectively. Similar absorption spectra have been reported for Fe^{2+} forms of nonsymbiotic rice hemoglobin,[20] cytoglobins,[21]

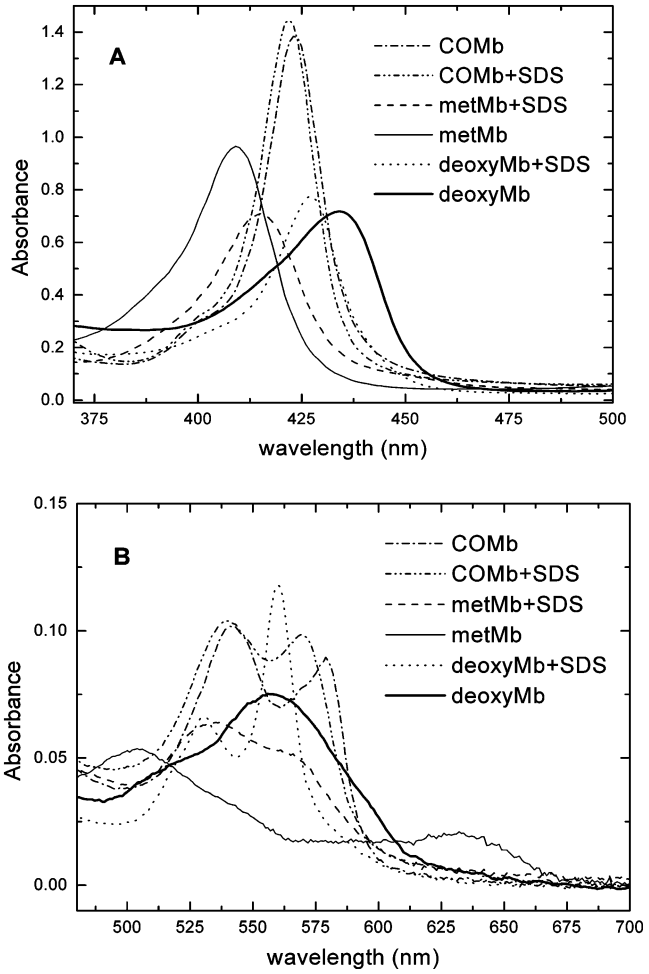

Figure 1. Steady-state optical spectra of met-, deoxy- and CO-bound Mb in the absence and presence of SDS. Experimental conditions: 5 μM Mb in 50 mM Tris buffer, pH 7.5. SDS concentration was 400 μM for metMb and 700 μM for deoxy- and CO-bound Mb. The Soret region is shown in panel A and the visible region in panel B.

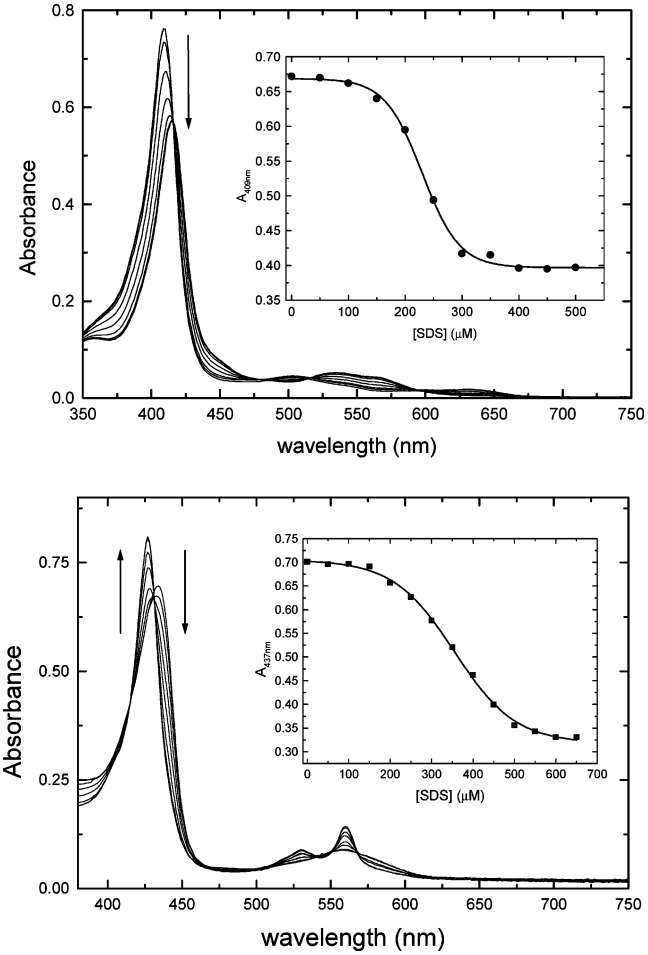

Figure 2. Equilibrium unfolding curve of metMb (upper panel) and deoxyMb (bottom panel) derived from absorbance changes at 409 and 437 nm, respectively. The solid lines are fits to the data using eq 1. The fitting parameters are $\theta_N = 0.670$, $m_N = -0.003$, $\theta_U = 0.405$, $m_U = -0.001$, $\Delta G_{H_2O} = 4.6$ kcal mol^{-1} and $-m = 18.1$ kcal mol^{-1} M^{-1} for metMb and $\theta_N = 0.705$, $m_N = -0.007$, $\theta_U = 0.32$, $m_U = -0.005$, $\Delta G_{H_2O} = 3.3$ kcal mol^{-1} and $-m = 8.1$ kcal mol^{-1} M^{-1} for deoxyMb. Experimental conditions: 5 μM Mb in 50 mM Tris buffer, pH 7.5.

and neuroglobins,[22] and are characteristic of six-coordinate low-spin Fe^{2+} heme with two histidine residues at the axial ligation positions. Increasing the SDS concentration higher than 800 μM SDS resulted in additional spectral changes that corresponded to the presence of high-spin five-coordinate heme, likely due to additional protein unfolding (data not shown). Addition of CO to deoxyMb in the presence of 700 μM results in a spectrum with a Soret band located at 422 nm and Q-bands located at 540 and 570 nm. An overlay of the CO-bound Mb spectrum in the absence and presence of SDS shows only minor changes in the position of the Soret band and more pronounced shifts in the positions of Q-bands, which are sensitive to the heme environment. In particular, the addition of surfactant causes an ~9 nm blue shift of the α band, going from 579 to 570 nm.

Figure 2 displays SDS titration curves of met- and deoxyMb. Data were fitted using a two-state unfolding model (eq 1), and the extrapolated parameters (C_m, ΔG_{H_2O}, and m_G) are listed in Table 1. The unfolding transition occurs at ~260 μM and ~350 μM SDS for met- and deoxyMb, respectively. The free energy change associated with the unfolding transition is comparable for met- and deoxyMb ($\Delta G_{H_2O} = 4.8$ kcal mol^{-1} and 3.9 kcal mol^{-1}), whereas the $-m$ value is nearly two times higher for metMb than for deoxyMb. The transition between native Mb to six-coordinate low-spin Mb is completed at ~350 μM SDS and at ~700 μM SDS for met- and deoxyMb, respectively. In distilled water, the cmc value for SDS was reported to be 8.27 mM, but is known to decrease in the presence of electrolytes.[23] For buffered solutions at neutral pH, the cmc value was determined to be ~2.6 mM.[24] Hence, it is likely that SDS monomers act as the denaturant. The transition was completed at an [SDS]/[Mb] molar ratio of ~70 and ~120 for met- and deoxyMb, respectively.

Table 1. C_m, ΔG_{H_2O}, and $-m_G$ Values of SDS-Induced Unfolding of metMb and deoxyMb Determined from Absorbance Changes at 409 and 437 nm, Respectively[a]

	C_m (mM)	ΔG_{H_2O} (kcal mol^{-1})	$-m$ (kcal mol^{-1}/mM)
metMb	0.26 ± 0.02	4.8 ± 1.1	17.4 ± 2.9
deoxyMb	0.35 ± 0.02	3.9 ± 1.3	9.9 ± 2.6

[a] Each reported value is the average value of three independent measurements.

From the titration of deoxyMb in the presence of 700 μM SDS with CO (Figure 3), the CO binding constant (K_a) was determined to be 4.0×10^4 M^{-1}. Competition with the internal histidine ligand decreases the affinity for CO, and the observed binding constant can be expressed as

$$K_a = \frac{K_{CO,five}}{1 + K_{His}} \quad (6)$$

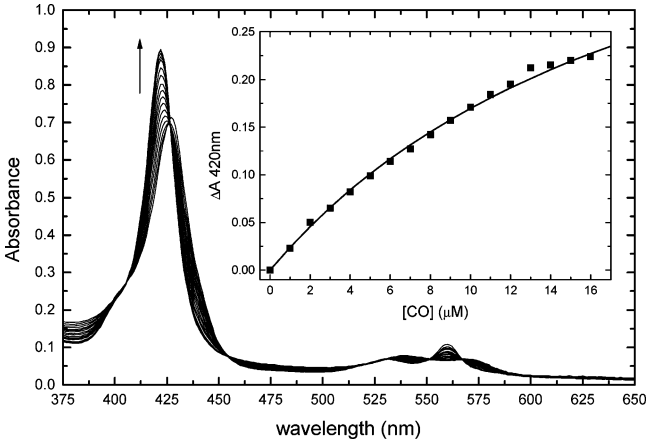

Figure 3. UV−vis spectra following CO binding to Mb in the presence of 700 μM SDS. Spectra were recorded in 50 mM Tris buffer, pH 7.5, at 20 °C. Inset shows the plot of the absorbance change at 420 nm vs [CO]. The solid line represents the fit according to eq 2.

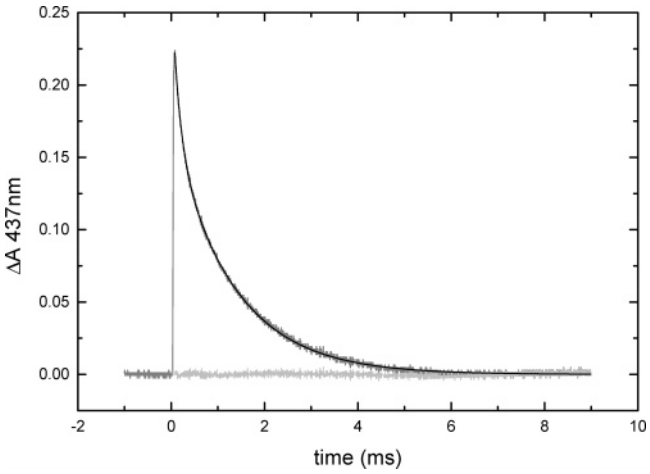

Figure 4. Single wavelength absorption trace for CO−Mb detected at 437 nm (maximum in the equilibrium difference spectra deoxyMb minus COMb). Experimental conditions: 5 μM Mb in 50 mM Tris buffer, pH 7.5, and 400 μM SDS. Black line represents double exponential fit to the data, and the residual is shown in light gray.

where $K_{CO,five}$ and K_{His} represent equilibrium constants for CO and histidine binding to five-coordinate Mb, respectively. Using the $K_{CO,five}$ previously determined for CO binding to heme model complexes in aqueous solution ($K_{CO,five} = 4.0 \times 10^8$ M^{-1}),[26] the His binding constant was estimated to be 1.0×10^4 M^{-1}. The value observed here is in agreement with previous observations that the affinity of Fe^{2+} heme for the second intramolecular imidazole ligand is significantly reduced in hemoprotein models.[25]

Figure 4 shows a flash photolysis trace for CO rebinding to deoxyMb at 350 μM SDS recorded at 437 nm. CO rebinding exhibits a double exponential decay, with the lifetime of the fast phase to be ~0.14 ms at 1mM CO. The lifetime of the slower phase is roughly 10 times slower ($\tau \approx 1.4$ ms). Traces recorded at 420 and 437 nm, which are the minimum and maximum of the equilibrium difference spectrum (deoxyMb−SDS minus COMb−SDS), show matching rate constants. The rate constants increase with increasing CO concentration and are attributed to CO binding (data not shown). The relative amplitudes of the fast and slow phase depend on SDS concentration, as shown in Figure 5. Below 300 μM SDS, CO rebinding occurs as a single-exponential process with a lifetime of 1.4 ms. In the concentration range between 300 μM and 800 μM, the rebinding process is biphasic. The lifetime of the fast

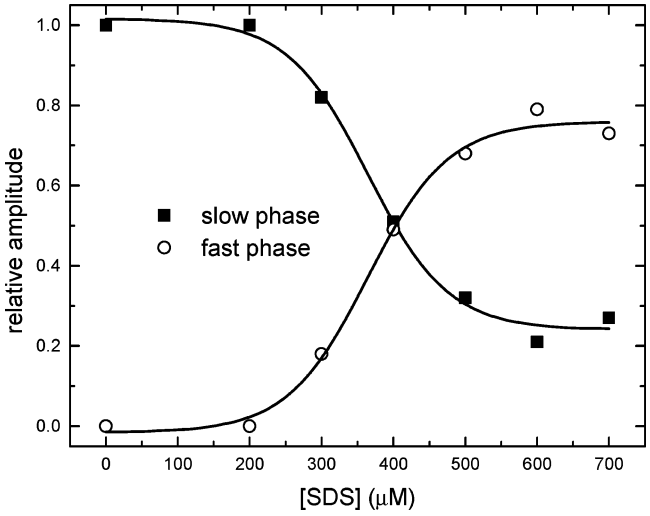

Figure 5. Relative amplitudes of the two phases observed during CO rebinding as a function of [SDS]. The amplitudes of the fast phase ($\tau = 0.14$ ms) are shown as open circles, and the amplitudes for the slow phase ($\tau = 1.5$ ms) are shown as solid squares. The transition midpoint ($C_m = 0.36 \pm 0.02$ mM) was obtained from the fit to the sigmoid equation (solid line).

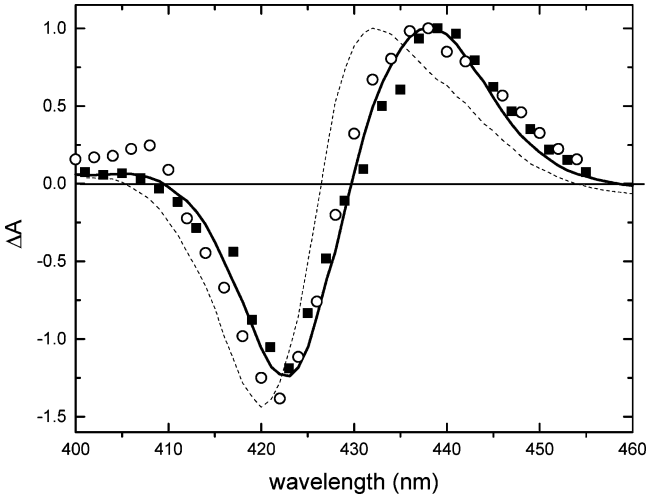

Figure 6. Equilibrium and transient difference spectra of deoxyMb minus CO Mb in the presence and absence of SDS. Solid line: equilibrium difference spectrum constructed by subtracting the CO Mb spectrum from deoxyMb spectrum. Dashed line: equilibrium difference spectrum in the presence of 700 μM SDS. Remaining spectra are kinetic difference spectra constructed from various single wavelength transient absorption traces. Spectra are postflash CO Mb (solid squares) and CO Mb-SDS (open circles).

and slow phase remain constant, whereas the relative amplitude of the fast phase increases as a function of SDS concentration, and the amplitude of the slow phase decreases. A sigmoidal fit of the plot of relative amplitudes as a function of SDS concentration provides the midpoint value ($C_m = 0.36 \pm 0.02$ mM), which matches the result from the steady-state UV−vis absorption spectra. Above 800 μM SDS, the rate constant for both phases further increases, likely because of the additional protein unfolding.

Laser flash photolysis of COMb in the presence of 700 μM SDS results in the formation of a five-coordinate high-spin heme as judged from the transient difference spectrum shown in Figure 6. The spectrum recorded 20 μs after photolysis exhibits a maximum at 438 nm, a minimum at 422 nm, an isosbestic point at 429 nm, and closely resembles the transient difference spectrum for CO photodissociation from native Mb as well as

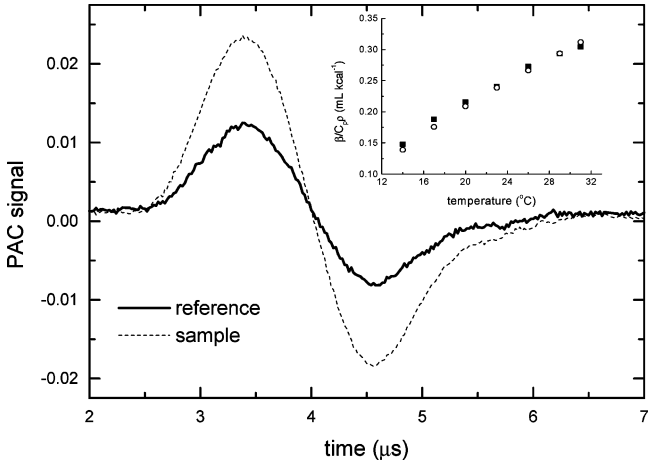

Figure 7. Overlay of the acoustic trace of CO dissociation from deoxyMb and the acoustic trace for the reference compound in 700 μM SDS and 50 mM Tris, pH 7.5, measured at 20 °C. The absorbance of the reference compound matched the absorbance of sample at the excitation wavelength ($A_{532nm} = 0.15 \pm 0.02$). The inset shows the ($\beta/C_p\rho$) values for reference compound in distilled water (open circles) and in 700 μM SDS and 50 mM Tris, pH 7.5 (solid squares) in the temperature range from 14 to 30 °C.

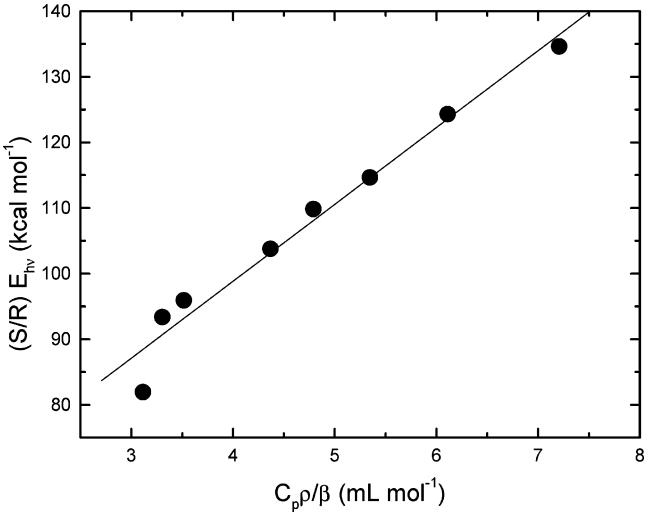

Figure 8. Plot of $(S/R)E_{h\nu}$ versus $C_p\rho/\beta$ for CO photodissociation from deoxyMb in the presence of 700 μM SDS. The volume and enthalpy changes coupled to CO dissociation from Mb were determined from the slope and the intercept of the linear fit, respectively (see text for details).

the equilibrium difference spectrum of deoxyMb minus COMb. On the other hand, the transient spectrum is distinct from that of the equilibrium difference spectrum of deoxyMb−SDS minus COMb−SDS, indicating no histidine rebinding within 20 μs.

Acoustic traces for CO dissociation from the SDS−Mb complex and the reference compound are shown in Figure 7. Fe(III) tetrakis(4-sulfonatophenyl)porphyrine (Fe4SP) was used as reference, since this molecule does not undergo any photochemistry and releases absorbed energy in the form of heat back to the solvent with a quantum yield of unity. Acoustic traces overlay in phase, indicating the absence of volume and enthalpy changes taking place between ~50 ns and ~10 μs. However, the larger amplitude of the sample acoustic wave relative to that of the reference compound points out the presence of volume and enthalpy changes taking place within ~50 ns. According to eqs 3−5, the reaction volume change and the amount of heat released to the solution were determined from a plot of $(S/R)E_h\nu$ versus $C_p\rho/\beta$ (Figure 8). To establish these values for solutions of 700 μM SDS in 50 mM Tris, pH 7.5, the amplitudes of the acoustic waves were obtained for the reference compound in the SDS solution in the temperature range between 15 and 30 °C, then compared to those for distilled water.[27] Calculated ($\beta/C_p\rho$) values are shown in Figure 7, inset. From a linear fit of the data in Figure 8, the volume change associated with ligand dissociation from the SDS−Mb complex is estimated to be 8.6 ± 0.6 mL mol^{-1} and the amount of heat released into the solution to be 50 ± 3 kcal mol^{-1}, using $\Phi = 1$ for CO photodissociation from Mb. The enthalpy change for CO photodissociation is calculated to be 4 ± 3 kcal mol^{-1}.

Discussion

In this study, we have investigated the interactions of the anionic surfactant SDS with horse heart myoglobin. At a concentration range below the cmc, SDS binding to Mb results in the accumulation of an equilibrium intermediate state with altered heme ligation. Steady-state absorption spectra reveal that the heme iron is low-spin six-coordinate, likely having the distal His residue as the sixth ligand in both metMb and deoxyMb forms. Such perturbations by SDS on metMb have been reported by Tofani et al.,[14] and analogous effects of SDS have been previously observed for other heme proteins such as hemoglobin and cytochrome *c*.[9−13] For example, previously reported steady-state fluorescence and CD studies have demonstrated that SDS binding to metMb is associated with changes in the tertiary and secondary structure of metMb.[14,34] Specifically, fluorescence emission from the two tryptophane residues (Trp7 and Trp14) progressively increases with increasing SDS (i.e., from 100 μM SDS to 700 μM SDS), and an additional increase in emission intensity was observed above ~1500 μM, in agreement with further unfolding of the protein.[14] Changes in the secondary structure due to SDS binding were also examined by CD spectroscopy showing that in the presence of 17 mM SDS the CD signal at 220 nm decreases approximately 20% relative to native Mb.[34]

To further characterize the SDS-induced equilibrium intermediate, we have determined the equilibrium unfolding parameters ΔG_{H_2O}, *m*, and C_m. In the case of metMb, the midpoint of the transition between the native high-spin five-coordinate to low-spin six-coordinate intermediate occurs at SDS concentrations of ~0.26 mM. For deoxyMb, the midpoint occurs at ~0.35 mM SDS, suggesting increased stability of deoxyMb toward unfolding. However, from analysis of the denaturation curves, the ΔG_{H_2O} was extrapolated to be the same, within experimental error, for both oxidation states ($\Delta G_{H_2O} = 4.8 \pm 1.1$ kcal mol^{-1} for metMb and $\Delta G_{H_2O} = 3.9 \pm 1.3$ kcal mol^{-1} for deoxyMb). These values are somewhat smaller than that determined for guanidine hydrochloride-induced myoglobin unfolding ($\Delta G_{H_2O} \approx 5.7$ kcal mol^{-1} for metMb and 7.2 kcal mol^{-1} for deoxyMb) suggesting that the SDS induced bis histidine met- and deoxy-intermediates do not adopt a random-coil conformation.[28]

On the other hand, a smaller $-m$ value is observed for deoxyMb than for metMb because of a higher degree of cooperativity in the metMb transition. The *m* parameter was proposed to correlate strongly with the amount of protein surface exposed to the solvent upon unfolding,[29] and indeed, small changes in the *m* value have been accounted for by significant changes in surface area exposed in the unfolded form.[30] In the native state, met- and deoxyMb adopt very similar structures as judged from X-ray studies. Changes in the *m* parameter therefore reflect differences in accessible surface area between met- and deoxyMb unfolding intermediates. In fact, the smaller

value determined for deoxyMb indicates a more compact intermediate structure relative to metMb. We speculate that charge neutralization and the hydrophobic nature of the Fe^{2+} heme may contribute to the more compact structure of the SDS-induced unfolding intermediate.

Results of laser flash photolysis show that the CO rebinding kinetics to the Mb−SDS complex are strongly dependent on the surfactant concentration. Since the transient difference spectrum recorded 20 μs after ligand dissociation is superimposable to that of CO photodissociation from native Mb, it is clear that ligand photolysis results in the formation a five-coordinate high-spin heme. Subsequent ligand rebinding is biphasic in the concentration range from 300 μM to 800 μM SDS. The lifetime of the fast phase was determined to be ~0.14 ms, whereas the slow phase exhibits a lifetime of 1.4 ms at 1 mM CO, which is similar to the lifetime observed for native Mb ($\tau = 1.7$ ms). These data suggest that myoglobin exists in at least two distinct conformations: a "nativelike" conformation with restricted access to the heme pocket and an "open" conformation with the heme group being more exposed to the solvent. Increasing the SDS concentration results in an equilibrium shift that favors the "open" conformation. Relative to the data presented in Figure 2, bottom panel, which shows that the transition between five-coordinate low-spin to six-coordinate high-spin deoxyMb is complete at 700 μM SDS, the CO rebinding data indicates that there is still a population of Mb which exhibits slow CO rebinding in the presence of 700 μM SDS. This indicates that at this SDS concentration there is a small fraction of SDS−Mb complex with bis histidine ligation which, however, retains the "nativelike conformation".

The transition from the "nativelike" Mb conformation to the "open" conformation in the SDS−Mb complex is further confirmed by our photoacoustic data showing that CO photodissociation from the SDS−Mb complex is associated with a prompt (<50 ns) expansion of 8.6 ± 0.6 mL mol^{-1} and an enthalpy change of ~4 kcal mol^{-1}. No additional kinetics were observed between ~50 ns and ~5 μs. From the previous studies, the enthalpy of the Fe−CO bond was determined to be on the order of ~17 kcal mol^{-1}. The volume change associated with CO dissociation from heme model complexes was found to be ~15 mL mol^{-1} and was attributed to the cleavage of the CO−Fe bond and the low-spin to high-spin heme transition.[31] Smaller volume and enthalpy changes observed for CO dissociation from the Mb−SDS complex suggest that another process may occur upon ligand dissociation. This process is expected to be exothermic ($\Delta H \approx 13$ kcal mol^{-1}) and have a negative volume change ($\Delta V \approx -6$ mL mol^{-1}) to compensate for the observed smaller volume and enthalpy changes. Taking into account that the transient absorption difference spectrum does not indicate any changes in heme coordination within 20 μs after photolysis, we associate this process to a protein relaxation after the low-spin to high-spin heme transition. These data are in agreement with the previous transient absorption studies on CO photodissociation and rebinding to chelated heme model complexes and heme proteins, which have shown that Fe−CO bond dissociation and the associated low-spin six-coordinate to high-spin five-coordinate heme iron transition occurs in <1 ns. Subsequent ligand rebinding takes place on the microsecond time scale and proceeds predominantly through a direct association mechanism.[36]

The acoustic data for CO photolysis from the Mb−SDS complex are in contrast to those determined for native myoglobin by Peters and co-workers.[32,33] These authors reported that ligand dissociation is coupled to a prompt volume contraction (τ < 10 ns) that is followed by a volume expansion with an ~700 ns lifetime. The second process was attributed to ligand migration from the inside of the protein to bulk water. In fact, ligand escape pathways in Mb were identified using various computational and experimental techniques including cryogenic and time-resolved Laue X-ray diffraction.[34−38] Immediately after the CO photodissociation, the ligand is docked in the distal pocket of the heme site and escapes from the protein matrix through hydrophobic Xe binding cavities.[39] Our data show that CO dissociation from the Mb−SDS complex occurs faster than from native Mb by at least a factor of 10, indicating that SDS binding to Mb results in significant changes in the heme binding site conformation. It was previously reported that two binding sets exist in the protein−SDS complex, the first involving electrostatic interactions and the second being hydrophobic in nature. Tofani et al.[14] proposed that SDS interactions with metMb include surfactant monomers binding to positively charged lysines, which leads to disruption of salt bridges between lysine residues from helix E and glutamic and aspartic acid residues from helix A. An increase in protein flexibility allows the distal histidine to move closer to the heme iron and form the intermediate with bis histidine ligation. However, it would seem unlikely that simple alterations of the hydrogen bond network on the protein surface can account for the observed acceleration of CO dissociation and rebinding kinetics in deoxyMb−SDS. It is more likely that the increase in protein flexibility due to electrostatic interactions between sulfate groups and lysine residues allows penetration of surfactant hydrophobic tails into the heme binding site, causing changes in hydrophobic interactions in the distal pocket. Such changes in the distal pocket, which is the primary docking site on the CO escape pathway, may open a more direct pathway for ligand escape and account for the observed fast CO dissociation and rebinding.

Acknowledgment. This work was supported by the National Science Foundation/EPSCoR (to Marshall University), American Heart Association (AHA 025537 to R.W.L.) and the National Science Foundation (NSF MCB0317334 to R.W.L.).

References and Notes

(1) Tanford, C.; Reynolds, J. A. *Biochim. Biophys. Acta* **1976**, *457*, 133−170.
(2) Jones, M. N.; Manley, J. P. *J. Chem. Soc., Faraday Trans.* **1980**, *76*, 654
(3) Sun, C. H.; Yang, J.; Wu, X.; Huang, X.; Wang, F.; Liu, S. *Biophys. J.* **2005**, *88*, 3518−3524.
(4) Durchschlag, H.; Tiefenbach, K.-J.; Gebauer, S.; Jaenicke, R. *J. Mol. Struct.* **2001**, *563*−564, 449−455.
(5) Jones, M. N.; Manledy, P. J. *J. Chem. Soc., Faraday Trans.* **1979**, *75*, 1736.
(6) Moren, A. K.; Khan, A. *Langmuir* **1995**, *11*, 3636−3643.
(7) Turro, N. J.; Lei, X.-G.; Ananthapadmanabhan, K. P.; Aronson, M. *Langmuir* **1995**, *11*, 2525−2533.
(8) Guo, X. H.; Zhao, N. M.; Chen, S. H.; Teixeira, J. *Biopolymers* **1990**, *29*, 335−346.
(9) Das, T. K.; Mazumdar, S.; Mitra, S. *Eur. J. Biochem.* **1998**, *254*, 662−670.
(10) Bertinini, I.; Turano, P.; Vasos, P. R.; Bondon, A.; Chevance, S.; Simonneaux G. *J. Mol. Biol.* **2004**, *336*, 489−496.
(11) Xu, Q.; Keiderling, T. A. *Protein Sci.* **2004**, *13*, 2949−2959.
(12) Moosavi-Movahedi, A. A.; Chamani, J.; Goto, Y.; Hakimelahi, G. H. *J. Biochem.* **2003**, *133*, 93−102.
(13) Sau, A. K.; Currell, D.; Mazumdar, S.; Mitra, S. *Biophys. Chem.* **2002**, *98*, 267−273.
(14) Tofani, L.; Feis, A.; Snoke, R. E.; Berti, D.; Baglioni, P.; Smulevich, G. *Biophys. J.* **2004**, *87*, 1186−1195.
(15) Anderson, J. L. R.; Chapman, S. K. *Dalton Trans.* **2005**, 13−24.
(16) Santoro, M. M.; Bolen, D. W. *Biochemistry* **1988**, *27*, 8063−8068.
(17) Miksovska, J.; Larsen, R. W. in *Methods in Enzymology*; Marriott, G., Parker, I., Eds.; Biophotonics Series 360; Academic Press: New York, 2003; Part A, pp 302−329.

(18) Schulenber, P. J.; Gartner, W.; Braslavsky, S. E. *J. Phys. Chem.* **1995**, *99*, 9617−9624.
(19) Braslavsky, S. E.; Heibel, G. E. *Chem. Rev.* **1992**, *92*, 1381−1410.
(20) Duff, S. M. G.; Wittenberg J. B.; Hill, R. D. *J. Biol. Chem.* **1997**, *272*, 16746−16752.
(21) Dewilde, S.; Kiger, L.; Burmester, T.; Hankeln, T.; Baudin-Creuza, V.; Aerts, T.; Marden, M. C.; Caubergs, R.; Moens, L. *J. Biol. Chem.* **2001**, *276*, 38949−38955.
(22) Sawai, H.; Kawada, N.; Yoshizato, K.; Nakajima, H.; Aono, S.; Shiro, Y. *Biochemistry* **2003**, *42*, 5133−5142.
(23) Mukerjee, P.; Mesels, K. J. National Standards Data Service; National Bureau of Standards, Washington, DC, 1971.
(24) Brito, R. M. M.; Vaz, W. L. C. *Anal. Biochem.* **1986**, *152*, 250−255.
(25) Rougee, M.; Brault, D. *Biochemistry* **1975**, *14*, 4100−4106.
(26) Traylor, T. G.; Brzinis, A. P. *Proc. Natl. Acad. Sci. U.S.A.* **1980**, *77*, 3171−3175.
(27) Wintung-Stafshede, P. *Biochim. Biophys. Acta* **1999**, *1432*, 401−405.
(28) Myers, J. K.; Pace, C. N.; Scholtz, J. M. *Protein Sci.* **1995**, *4*, 2138−2148.
(29) Alonso, D. O.; Dill, K. A. *Biochemistry* **1991**, *30*, 5974−5985.
(30) Miksovska, J.; Norstrom, J.; Larsen, R. W. *Inorg. Chem.* **2005**, *44*, 1006−1014.
(31) Westrick, J. A.; Peters, K. S. *Biophys. Chem.* **1990**, *37*, 73−79.
(32) Westrick, J. A.; Peters, K. S. *Biochemistry* **1990**, *29*, 6741−6746.
(33) Srajer, V.; Teng, T.-Y.; Ursby, T.; Pradervand, C.; Ren, Z.; Adachi, S.; Schildkamp, W.; Bourgeois, D.; Wulff, M.; Moffat, K. *Science* **1996**, *274*, 1726−1729.
(34) Mattice, W. L.; Riser, J. M.; Clark, D. S. *Biochemistry* **1976**, *15*, 4264−4272.
(35) Taylor, T. G. *Acc. Chem. Res.* **1981**, *14*, 102−109.
(36) Srajer, V.; Ren, Z.; Teng, T.-Y.; Ursby, T.; Bourgeois, D.; Pradervand, C.; Schildkamp, W.; Wulff, M.; Moffat, K. *Biochemistry* **2001**, *40*, 13802−13815.
(37) Lamb, D. C.; Nienhaus, K.; Arcovito, A.; Draghi, F.; Miele, A. E.; Brunori, M.; Nienhaus, G. U. *J. Biol. Chem.* **2002**, *277*, 11636−11644.
(38) Agmon, N. *Biophys. J.* **2004**, *87*, 1537−1534.
(39) Scott, E. E.; Gibson, Q. H. *Biochemistry* **1997**, *36*, 11909−11917.

BM0506703